Probing the Flexibility of the Bacterial Reaction Center: The Wild-Type Protein Is More Rigid Than Two Site-Specific Mutants

Sophie Sacquin-Mora,[‡] Pierre Sebban,[§] Valérie Derrien,[§] Bernhard Frick,[||] Richard Lavery,[‡] and Christiane Alba-Simionesco*[,§]

Laboratoire de Biochimie Théorique, CNRS UPR 9080, Institut de Biologie Physico-Chimique, 13 rue Pierre et Marie Curie, 75005 Paris, France, Laboratoire de Chimie Physique, CNRS UMR 8000, Bâtiment 349, Université de Paris Sud, 91405 Orsay, France, and Institut Laue-Langevin, 6, rue Horowitz, F-38042 Grenoble, France

Received March 5, 2007; Revised Manuscript Received October 9, 2007

ABSTRACT: Experimental and theoretical studies have stressed the importance of flexibility for protein function. However, more local studies of protein dynamics, using temperature factors from crystallographic data or elastic models of protein mechanics, suggest that active sites are among the most rigid parts of proteins. We have used quasielastic neutron scattering to study the native reaction center protein from the purple bacterium *Rhodobacter sphaeroides*, over a temperature range of 4−260 K, in parallel with two nonfunctional mutants both carrying the mutations L212Glu/L213Asp → Ala/Ala (one mutant carrying, in addition, the M249Ala → Tyr mutation). The so-called dynamical transition temperature, T_d, remains the same for the three proteins around 230 K. Below T_d the mean square displacement, $\langle u^2 \rangle$, and the dynamical structure factor, $S(Q,\omega)$, as measured respectively by backscattering and time-of-flight techniques are identical. However, we report that above T_d, where anharmonicity and diffusive motions take place, the native protein is more rigid than the two nonfunctional mutants. The higher flexibility of both mutant proteins is demonstrated by either their higher $\langle u^2 \rangle$ values or the notable quasielastic broadening of $S(Q,\omega)$ that reveals the diffusive nature of the motions involved. Remarkably, we demonstrate here that in proteins, point genetic mutations may notably affect the overall protein dynamics, and this effect can be quantified by neutron scattering. Our results suggest a new direction of investigation for further understanding of the relationship between fast dynamics and activity in proteins. Brownian dynamics simulations we have carried out are consistent with the neutron experiments, suggesting that a rigid core within the native protein is specifically softened by distant point mutations. L212Glu, which is systematically conserved in all photosynthetic bacteria, seems to be one of the key residues that exerts a distant control over the rigidity of the core of the protein.

Protein function clearly depends not only on structure but also on flexibility (*1*−*4*). The complex nature of protein flexibility has been demonstrated by a variety of experimental techniques including Mössbauer spectroscopy (*4*), light scattering (*5*), and neutron scattering (*6*−*9*) and also by molecular dynamics simulations (*2*, *10*, *11*). All these studies have stressed the importance of the diffusive motions present at room temperature, enabling a protein to overcome the energetic barriers between neighboring conformational substates. The importance of these motions has led some authors to conclude that enzyme active sites should be the most flexible parts of proteins (*3*).

Another picture has emerged from studies of the heterogeneous nature of the internal vibrational mechanics of proteins. Data on this type of flexibility can be obtained from the temperature factors resulting from crystallographic studies, from simulations using elastic protein models, and from potential energy landscape descriptions. In contrast to the more global studies mentioned above, these results rather suggest that active sites are among the most rigid parts of proteins (*12*−*18*).

We have addressed this question and demonstrated here that, *a contrario* to the former belief, in the case of redox proteins at least, an excessive flexibility can be related to an absence of activity (absence of proton delivery). For that purpose we have carried out a combined experimental and theoretical study on the wild-type and on two nonfunctional mutants of the bacterial photosynthetic reaction center (RC[1]) from the purple bacterium *Rhodobacter* (*R.*) *sphaeroides*. RC, an ancestor of modern photosystem II from higher photosynthetic organisms, converts light into chemical free energy via coupled electron and proton transfers (*19*−*21*). The RC complex is composed of three subunits (L, M, and H) with

* Corresponding author. Tel: +33 1 69 15 66 94. Fax: +33 1 69 15 61 88. E-mail: chalba@lcp.u-psud.fr.

[‡] Institut de Biologie Physico-Chimique.

[§] Université de Paris Sud.

[||] Institut Laue-Langevin.

[1] Abbreviations: AA, L212Glu/L213Asp → Ala/Ala mutant; AA+Y, L212Glu/L213Asp → Ala/Ala + M249Ala → Tyr mutant; HEPES, 4-(2-hydroxyethyl)-1-piperazineethanesulfonic acid, ILL, Institute Laue-Langevin; P, primary electron donor, a noncovalently linked bacteriochlorophyll dimer; Q_A and Q_B, primary and secondary quinones; *R.*, *Rhodobacter*; RC, reaction center; $S(Q,\omega)$, dynamical structure factor; TOF, time of flight; Triton X-100, octylphenol polyethylene glycol ether, $\langle u^2 \rangle$, mean square displacement; UQ, ubiquinone, 2,3-dimethoxy-5-methyl-6-hexaisoprenyl-1-4-benzoquinone; WT, wild type.

10.1021/bi7004416 CCC: $37.00
Published on Web 12/04/2007

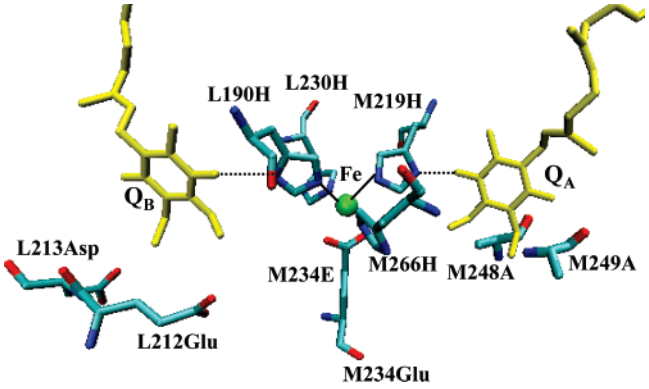

FIGURE 1: Structural region of the quinones in the RC from *R. sphaeroides* (pdb 1K6L) including the nonheme iron and its ligands, L190His, L230His, M219His, M266His, and M234Glu.

a total molecular weight of about 100 kDa. The helical transmembrane subunits L and M are related by an approximate 2-fold symmetry axis and contain ten cofactors arranged in two branches (termed A and B). Absorption of photons by the RC leads to the formation of the singlet electronic excited-state of lowest energy of a dimer of bacteriochlorophylls ("P*"). This strong reducing species initiates a charge separation across the cytoplasmic membrane between the oxidized P^+ and the first quinone acceptor, Q_A^-. The electron is then transferred to the secondary quinone, Q_B. Q_A and Q_B are both ubiquinone$_{10}$ molecules. After two photochemical events, Q_B is doubly reduced and doubly protonated as a dihydroquinone, Q_BH_2. Because of numerous structural (*22*−*25*) and functional studies (*19*, *21*) carried out on this important energy-converting protein, it is considered to be an excellent model for investigating the subtle molecular movements that accompany the functioning of bioenergetics membrane systems.

Point mutations in RC have been very useful in understanding the function of this protein (see for example refs *26*−*28*). Among the point mutations which block RC function, we have chosen to investigate the vibrational and dynamical properties of the double mutant L212Glu/L213Asp → Ala/Ala (hereafter termed AA) and of the similar nonfunctioning triple mutant AA + M249AY (hereafter termed AA+Y) (*29*). These two mutants are photosynthetically incompetent since removal of L212Glu and L213Asp results in a ∼1000 times reduction of, respectively, the second (*27*) and first (*28*) proton transfer to Q_B. The M249Ala → Tyr mutation does restore the stoichiometry of proton uptake induced by the Q_A^- and Q_B^- formations but does not restore the proton-transfer kinetics (which is only two times faster than that of the AA strain) to a level allowing the triple mutant to grow under photosynthetic conditions (*29*). M249Ala, which is structurally analogous to L213Asp, lies below Q_A at ∼18 Å from Q_B (see Figure 1).

Crystallographic studies of AA show that, although the mutations involve a reduction in side chain volume at the mutated sites, there are very limited changes in structure (the overall Cα rmsd between the WT and AA forms is only 0.1 Å) (*24*). The three-dimensional structure of the AA+Y mutant has not been resolved, but preliminary results (Pokkuluri, P.R., Laible, P.D., Deng, Y.L., Wong, T.N., Hanson, D.K., and Schiffer, M., unpublished data) and ref *29* show no significant changes compared to the AA mutant, even within the Q_A region. In the AA structure, the main modifications involve a slight opening up of the backbone loop (L207−L227) which sequesters Q_B. The Cα's of these residues move by 0.1−0.3 Å, culminating in an increase of the L209−L226 distance by almost 1 Å. A significant movement of Q_B (roughly 3.5 Å) is observed toward the site proximal to the nonheme iron, less than 1 Å from the position it occupies in the light-adapted form of the RC (*23*).

While these changes are certainly interesting, one would not expect them to have significant effects on the dynamics of a structure of this size (the RC contains a total of 848 amino acids). However, we show here using neutron scattering methods (measuring the mean square displacement, msd or $\langle u^2 \rangle$, and the dynamical structure factor, $S(Q,\omega)$ by backscattering and time-of-flight techniques) that the AA mutations in both mutants lead to similar increased overall mobility. Data on both mutants are superimposable and clearly differentiated from the WT above the dynamical transition temperature. Moreover, information derived from theoretical studies of residue-by-residue mechanical properties is consistent with this result and highlights the possible origin of these observations, namely a softening of the core of the protein centered on the nonheme iron and its ligands in both the AA and AA+Y mutants.

MATERIALS AND METHODS

Biochemical Techniques. The construction of the AA and AA+Y mutants have previously been described (*30*). The cells were grown in Erlenmeyer flasks filled to 50% of the total volume with malate yeast medium supplemented with kanamycin (20 μg/mL) and tetracycline (2 μg/mL). The cultures were grown in the darkness at 30 °C on a gyratory shaker (100 rpm). The RC purification from the WT and the mutants has previously been described (*31*).

For neutron scattering experiments, three cycles of concentration (∼10 times) followed by dilution with D_2O were achieved. Therefore replacement of H_2O by D_2O was completed to a ratio of ∼1000. The reaction centers were resuspended in buffer containing both the detergent Triton X-100 0.03% w/v and HEPES 10 mM, pD 7.93 (pH 7.5). This low concentration of detergent minimizes the possibility of free micelles formation.

Neutron Scattering. Neutron spectroscopy can give a detailed picture of how atoms or molecules move on the atomic scale in time and space. The spatial sensitivity (here from a few nanometers to a few angstroms) is of particular importance and distinguishes neutron spectroscopy from many other spectroscopic methods for time scales ranging between 0.1 ps and 1 ns. Here, neutron backscattering experiments were performed to an energy resolution of 1 meV. We focus on the elastic scattering intensity $I(Q,T,\omega=0)$ measured in the elastic fixed-window mode as a function of temperature from 2 to 280 K. The incoherent elastic intensity at a given scattering wave vector Q, $I(Q,T)$, decreases with increasing temperature, following the equation $I(T,Q) = I_0 \exp[-a(T)Q^2]$, where a is the average atomic mean-squared displacement, taken here to be $1/3\langle u^2 \rangle$. An effective $\langle u^2 \rangle$ on the nanosecond time scale is then extracted from the Q-dependence by fitting straight lines to $\ln(I/I_0)$ versus Q^2. Q was analyzed from 0.2 to 1.3 $Å^{-1}$, avoiding effects associated with the Bragg peaks of water (above 1.5 $Å^{-1}$), and the linear dependence of $\ln(I)$ as a function of Q^2 was

carefully checked, justifying the Gaussian approximation. The reader can find more details in the references where this analysis is well explained (*65*, 66). The wild-type and mutant proteins were produced in sufficient quantities for neutron scattering, extracted, and solubilized in detergent/water solutions. We used concentrations of 720 μM for the WT RC, 620 μM for the AA mutant, and 585 μM for the AA+Y mutant, with 30 mg mL^{-1} detergent (Triton X100). On the basis of the radius of gyration of the WT RC, 31.8 $\pm$ 0.1 Å, measured by small angle neutron scattering experiments (*32*), the protein occupies approximately 5.6% of the total volume of the solution (or about 9% belonging taking into account the detergent micelle). Replacement of H_2O by D_2O enables the dynamics of the hydrogen atoms of the protein to be measured independently of the solvent contribution. The high protein concentration achieved here, leads to a 67% contribution from the hydrogen atoms of the protein to the total scattering intensity. After the neutron experiments, the absorption spectra and the electron-transfer kinetics were checked for the three systems. We observed that these properties remained unaltered by the thermal treatment imposed by the neutron scattering experiments. Indeed, the steady state absorption spectra (280−900 nm) of the WT and mutants RC proteins could be superimposed to that of the same samples taken before the neutron experiments. Concerning the $P^+Q_A^-$ and $P^+Q_B^-$ charge recombination kinetics as well as the first and second electron-transfer kinetics between Q_A and Q_B, the rate constants were found identical within 10% to those measured before neutron experiments. For the TOF experiments, the spectra of the three samples were taken under the closest possible experimental conditions, leading to similar elastic intensity, the remaining differences, after all corrections, being due to slight differences in the illuminated area of the cell. Therefore, spectra normalized to this elastic intensity are plotted and compared to the instrumental resolution function obtained with the RC sample and to the buffer at the same temperature. The theoretical $S(Q,\omega)$ results from the deconvolution of the experimental data and the instrumental resolution function; $S(Q,\omega)$ can be decomposed into separate elastic, quasielastic, and inelastic components, where the elastic peak originates from neutrons undergoing no change in energy. The quasielastic line is attributed to the diffusive, rotational, or translational motions and consists of a broad band of intensity centered at ω=0. The inelastic component is related to the vibrational modes of the sample. The TOF experiments were carried out on the TOF spectrometer IN6 at the ILL with a wavelength λ = 5.1 Å The spectra are normalized by the intensity at ω=0 and compared to the instrumental resolution function measured at 11 K and to the buffer under the same conditions; the scattering wave vector Q is 1.5 Å^{-1}, ω is the energy transfer in meV (1 meV = 0.24 THz = 8 cm^{-1}). The three proteins were first cooled from room temperature down to low temperatures and then heated to the temperature of the measurement. The experiments were performed at four temperatures: 180 K (below T_d), 240 K and 270 K (above T_d), and 280 K (above the melting temperature of D_2O).

Our main goal here is the comparison of the native protein dynamics with that of its variants under the closest possible experimental conditions. We have chosen to not subtract the contribution of the buffer, since the latter remains almost

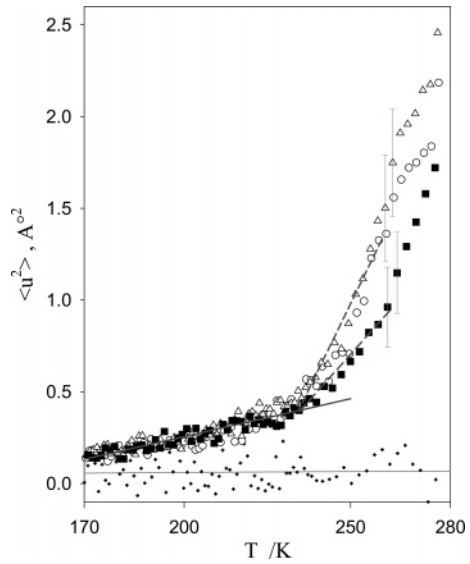

FIGURE 2: Temperature dependence of the mean square displacement $\langle u^2 \rangle$ from neutron backscattering for the wild-type (closed squares) and the AA (open circles) and AA+Y (open triangles) RC mutants from *R. sphaeroides*, compared to the buffer (D_2O, 0.1% Triton X-100 detergent, HEPES 10 mM, pD 7.93 (pH 7.5)). Error bars are only shown for the WT RC but are of similar magnitude for the mutant proteins. The dots correspond to the solvent and detergent alone measured and analyzed under the same conditions. The solid line is a linear fit of the lower temperature portion of $\langle u^2 \rangle$ common to all proteins, and dashed lines indicate the differing slopes of $\langle u^2 \rangle$ for the mutants and the WT above T_d, the dynamical transition temperature (approximately 230 K for all three proteins). This change is attributed to the onset of anharmonicity and diffusive dynamics. Above T_d, until the melting temperature (277 K in D_2O), larger amplitude motions, corresponding to increased flexibility, are found for the mutated proteins.

constant in the T range of interest for the mean square displacement experiments (see Figure 2) up to the melting temperature of D_2O and does not contribute to any quasielastic scattering in the $S(Q,\omega)$ plotted in Figure 3.

Molecular Simulations. The simulations carried out here used a reduced protein model where each amino acid is represented by one pseudoatom located at the Cα position, and either one or two pseudoatoms representing the sidechains (with the exception of Gly) (*33*). All pseudoatoms lying closer than 9 Å were joined with quadratic springs having a common force constant of 0.6 kcal mol^{-1} Å^{-2}, a value slightly smaller than in one-point-per-residue coarse-grained models, which usually employ values around 1.0 kcal mol^{-1} Å^{-2} (*17*, *34*, *35*). This choice was made to offset the higher spring density of the multipoint amino acid representation.

The springs were taken to be relaxed in the corresponding crystallographic conformation of the protein. The crystallographic conformations were taken from the Protein Data Bank (*36*): pdb 1K6L for the WT RC and pdb 1K6N for the AA mutant of *R. sphaeroides* (*24*). As in our earlier studies, the prosthetic groups of the proteins were not taken into account, enabling the intrinsic mechanics of the protein structure to be studied. However, we note that, at least in the proteins studied previously, these groups had little influence on the results (*14*, *15*).

Brownian dynamics simulations of 500 ps were carried out on the WT RC and the AA mutant following the protocol described elsewhere (*14*). Effective force constants for

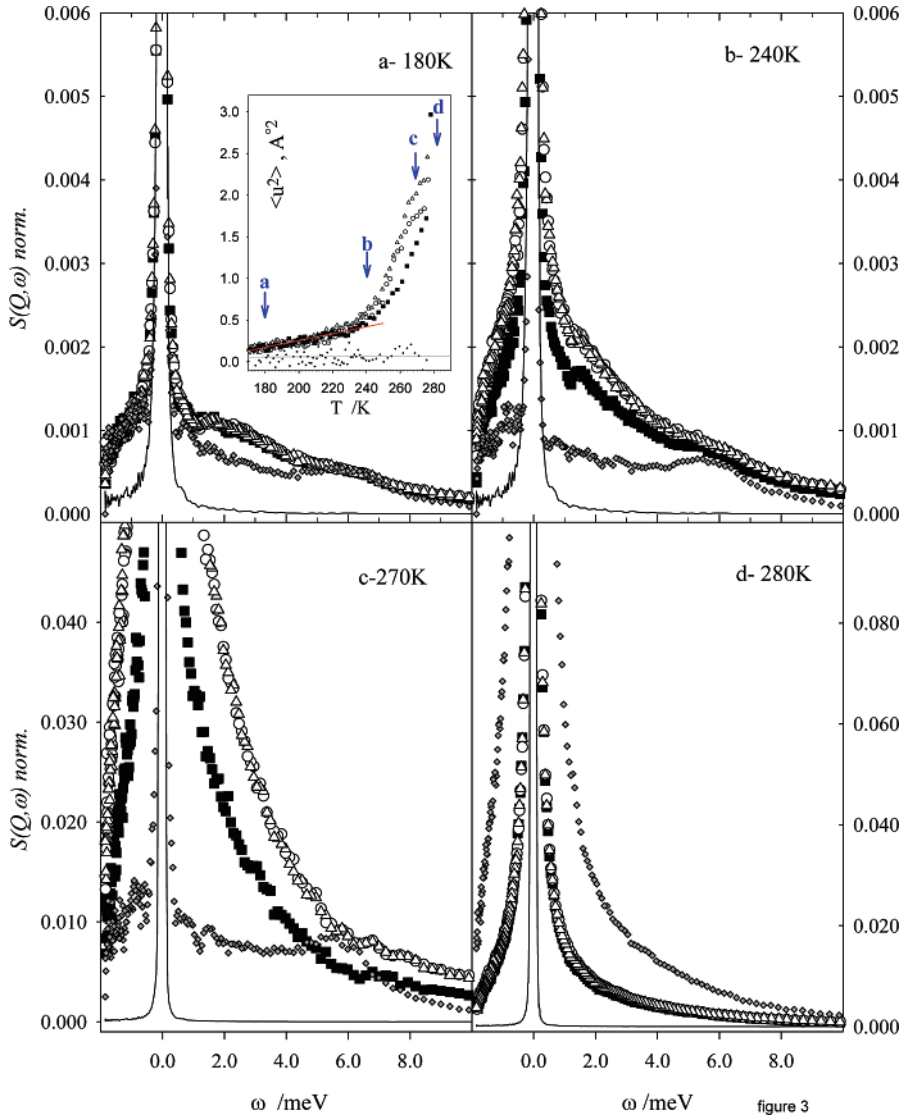

FIGURE 3: Incoherent dynamic structure factor $S(Q,\omega)$ of the wild-type RC and the two mutants from quasielastic neutron scattering on the TOF spectrometer IN6 at the ILL (Grenoble, France). Same symbols as in Figure 1: wild-type RC (closed squares), AA (open circles), and AA+Y (open triangles). The spectra are normalized by the intensity at ω=0 and compared to the instrumental resolution function (thin lines) obtained at 11 K and to the buffer (D_2O + detergent, gray diamonds); the scattering wave vector Q is 1.5 $Å^{-1}$, ω is the energy transfer in meV. (a) At a temperature of 180 K, the three systems are identical in their elastic and inelastic contributions. The shoulder observed around 6 meV corresponds to water and is also found in the buffer. At lower frequencies an extra peak (1.5 meV), the so-called Boson peak, appears equivalently in all proteins. (b) 240 K, above the dynamical transition temperature, quasielastic broadening takes place but is more pronounced for the mutants than for the WT protein, corresponding to faster diffusive motions in the mutants. (c) 270 K, as at 240 K, the two mutants display the much faster diffusive contributions than the WT protein. At this temperature the Boson peak is no longer seen. The buffer clearly does not contribute to the quasielastic part observed. (d) 280 K, above the melting temperature of D_2O, the dynamics of the three proteins are dominated by the motions of water molecules in the buffer. Inset: msd same as in Figure 2; the arrows indicate the values of the msd where the $S(Q,\omega)$ were measured.

displacing each pseudoatom i within the protein were then calculated from the positional fluctuations each particle as

$$k_i = \frac{1}{\langle (d_i - \langle d_i \rangle)^2 \rangle}$$

where $\langle\rangle$ denotes an average taken over the whole simulation and $d_i = \langle d_{ij} \rangle_{j^*}$ is the average distance from particle i to the other particles j in the protein (the sum over j* implies the exclusion of pseudoatoms belonging to residue i). The distances between the Cα pseudoatom of residue i and the Cα pseudoatoms of the adjacent residues i − 1 and i + 1 are also excluded. These exclusions correspond to virtually constant distances. The force constant k for each residue is calculated as the average of the force constants of all the pseudoatoms i forming this residue. We use the term rigidity profile to describe the ordered set of force constants for all the residues of a given protein.

RESULTS

We begin by considering neutron scattering applied to the WT RC and to the AA and AA+Y mutants of *R. sphaeroides* and measuring $S(Q,\omega)$, the dynamical structure factor (where Q is the scattering wave vector and ω the energy transfer), with two different techniques: backscattering (BS) and time-of-flight spectrometers (TOF), probing motions, respectively, faster than 4 ns and 30 ps. In both cases, the incoherent scattering of the RC dominates the spectra largely due to its

high hydrogen content, and therefore the self-correlation function is measured to a good approximation. However, the data also contain a contribution of the solvent, which remains almost constant in the temperature and frequency range of our investigations and is minimized by substituting H_2O by D_2O.

The first experiments carried out using the quasielastic backscattering technique on the IN16 spectrometer at the Institut Laue Langevin (Grenoble, France) are analyzed in terms of average mean square displacement (denoted $\langle u^2 \rangle$) of the atoms composing the protein as a function of temperature (with the dominant contribution coming from the hydrogen atoms of the proteins). Figure 2 shows that, in common with earlier studies of globular proteins (*37*), the WT and the mutant RCs show two regimes with a change in the slope of $\langle u^2 \rangle$ at a dynamical transition temperature, T_d, corresponding to the onset of diffusive movements (*3*). Indeed, up to $T_d \sim 230$ K, the $\langle u^2 \rangle$ values for the WT and the two mutant proteins are superimposed. In this T range, the quantum efficiency for the electron transfer of the WT protein was found reduced by 60% and finally canceled at 150 K (*38*).

This value of T_d, which is roughly the same for the three different RC proteins (which $\langle u^2 \rangle$ values are superimposed), lies within the range previously observed for other proteins (150 K → 240 K) with comparable energy resolution (*2*, *3*, *5*, *8*, *10*, *37*, *39*−*41*).

Above T_d, a striking difference is detected between $\langle u^2 \rangle$ measured for the WT and the mutants, with a distinctly higher slope for both mutants. This indicates that the nonfunctional mutants are globally more flexible than the WT protein above the transition temperature. The distinction is maintained above 260 K, until it becomes dominated by the melting of the solvent at 277 K. Such a distinction between dynamics of proteins of virtually identical mass and structure differing only by point mutation has not been reported so far.

The rigidity of a given protein is often described by a resilience parameter k (an effective mean force constant in N/m calculated from the reciprocal of the slope of the $\langle u^2 \rangle$ vs T), as proposed by Zaccai et al. (*8*): the system is softer, or considered less resilient, when the force constant is smaller. This is the case when the dynamical transition is reached. Below T_d, we have found, equally for the three proteins, a force constant of the order of 3.8 N/m at very low temperature (20−130 K) decreasing to 0.734 N/m as T increases up to T_d, with an average of 2.14 ± 0.43 N/m. Above T_d, in a T range of 230−260 K, the three proteins behave differently: the WT is characterized by a resilience of 0.125 ± 0.008 N/m whereas the two mutants k values are much less, 0.089N/m and 0.092 N/m, respectively, for the AA and the AA+Y mutants. These parameters are of the same order of magnitude than those of the literature (*42*, *43*) and in a good agreement with the purple membrane bacteriorhodopsin.

These results are confirmed by a second set of experiments using the TOF technique, which allow the protein dynamics to be observed under the same conditions but at a shorter time scale. These experiments were carried out on the IN6 TOF spectrometer at the ILL. The results are presented in Figure 3, a−d.

At 180 K, below T_d (as determined by the $\langle u^2 \rangle$ measurements), the incoherent dynamic structure factor $S(Q,\omega)$ spectra of the three proteins are superimposable. This is illustrated in Figure 3a, where the three systems are identical in their elastic and inelastic contributions. The shoulder observed at an energy transfer of ∼ 6 meV corresponds to water and appears in the solvent as well.

The rigidity of a solid at low temperature can be evaluated from its collective dynamics *via* its vibrational density of states (observed here with the TOF technique). At low frequencies (in the THz, or meV, range), amorphous solids exhibit a pronounced excess of vibrational states over the Debye level, an excess known as the boson peak (*44*−*51*). This boson peak is displayed equivalently here (Figure 3, a−d) for the three proteins around 1−3 meV, as already observed in many enzymes (*13*, *37*, *52*−*57*). This indicates that the presence of soft modes is not affected by the mutations. At 180 K the boson peak is dominated by internal dynamics since the solvent is frozen, but it is not sensitive enough to reflect the effect of the mutations.

We now describe the TOF results above T_d (Figure 3, b−d). The temperature dependence of the $S(Q,\omega)$ spectra is fully consistent with $\langle u^2 \rangle$ data of Figure 2, above the dynamical transition. The quasielastic broadening that takes place in the $S(Q,\omega)$ measurements above $T_d = 230$ K is different for the WT protein and for the two mutants, as seen in Figures 3b and 3c at 240 and 270 K, respectively. The $S(Q,\omega)$ spectra are undistinguishable for the two protein variants, both being much broader than the WT. This illustrates the fact that the increase in temperature affects not only the position of the modes (by shifting them to lower frequencies) but also reveals extra processes specifically taking part in the relaxation mechanism and the softening of the AA and AA+Y mutants (see Discussion). Above the melting temperature of the solvent at 280 K (Figure 3d), the dynamics of water molecule dominates the spectra and masks the differences between the proteins.

Above 265 K, the $\langle u^2 \rangle$ of the mutants remain almost constant at variance to that of the native RC. The relaxation processes involved here are no more detectable in the spectral window of the IN16 BS spectrometer, while a continuous change is measured in the IN6 TOF spectrometer and the dynamics of the two mutants still coincide at 270 K. It could be due to motions on intermediate time scale and/or reminiscent of the dynamics of particles in confining media. However, in this T-range the $\langle u^2 \rangle$ data are extracted from low values of the elastic intensity that might introduce large error bars. Similar situations were found in the literature (*58*, *59*).

In order to probe the structural origins of the increased flexibility in the mutant proteins, we carried out a theoretical analysis of the internal mechanics of the WT and mutant proteins. Using a technique previously applied to the study of the mechanics of enzymatic catalytic sites (*14*), we were able to obtain a residue-by-residue view of these mechanical properties This involves carrying out Brownian dynamics simulations on a coarse-grain representation of the proteins, related to Gaussian network models (*60*, *61*), with each amino acid represented by two to three points (*33*) and quadratic springs joining points falling below a fixed cutoff

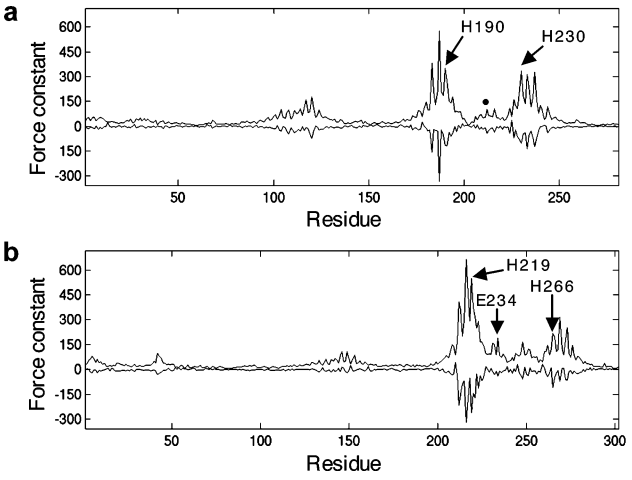

FIGURE 4: Effective force constant profiles (kcal mol^{-1} Å^{-2}) for the residues belonging to the RC: (a) L subunit; (b) M subunit. In each case, the upper line corresponds to the force constants for the WT RC. The largest values occur for functional residues surrounding the nonheme iron atom. The lower lines of each plot show the changes in the force constants when passing from the WT to the AA mutant. The overall increase in flexibility is again dominated by functional residues in the vicinity of the nonheme iron. The positions of the mutated residues within the sequence are shown by a black dot. Data for the H subunit are not shown, as the mutation is found to have no effect on the force constants of its residues.

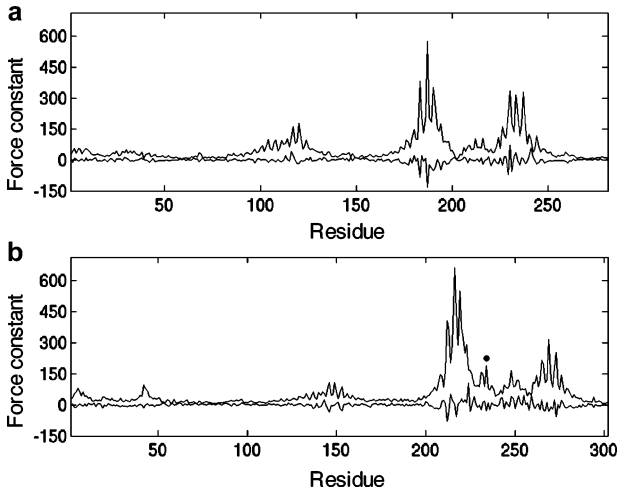

FIGURE 5: The influence of an artificial mutation M234Glu → Ala on the flexibility of the WT RC protein (modifying the pseudoatoms representing the mutated residue but not the protein conformation). The upper lines in plots a and b show the effective force constants for the L and M subunits (kcal mol^{-1} Å^{-2}). The lower lines show the changes in the force constants on passing from the WT to the artificial mutant. The mutated site is indicated by a black dot.

distance. The simulations were analyzed in terms of the fluctuations of the mean distance between each amino acid residue and the remaining residues of the protein. The inverse square of these fluctuations yields an effective force constant describing the ease of moving a given residue with respect to the overall protein structure. Studies with this approach support earlier work in showing that key functional residues are generally among the most rigid (*14*).

Figure 4 presents the results for the WT and AA forms of RC from the available structures of *R. sphaeroides* (pdb 1K6L for the WT RC and pdb 1K6N for the AA mutant of *R. sphaeroides* (*24*)). The force constant profile obtained for the WT RC reflects the pseudosymmetric structure of chains L and M (see the upper lines in Figures 4a and 4b). Regions around the nonheme iron center, notably L180−195, L225−240, M210−230, and M260−M275, exhibit the largest force constants, and the ligands directly binding the nonheme iron (L190His, L230His, M219His, M266His, and M234Glu) are among the highest values. It should be noted that comparing the curves of the inverse value of the B factors of the WT RC (obtained from the 1K6L pdb file) and the force constants determined here, leads to the same trends for the rigid parts of the protein. However, the force constants highlight more specifically the residues involved in this rigidity.

Turning to the lower curves in Figures 4a and 4b, we see that, as in the case of the neutron scattering studies, the AA mutation leads to significant local decreases in the force constants, corresponding to increased protein flexibility. The force constant profiles show that these changes occur in both the L and M chains, in the regions showing the highest force constants in the WT RC. Among other residues, M219His and L190His, thought to be involved in communication between the Q_A and Q_B sites (*26*, *62*, *63*), and M266His, whose mutation has been found to affect this communication (*64*), show notable increases in flexibility.

Artificially introducing the L212Glu/L213Asp → Ala/Ala mutations into the WT RC, without any other structural changes, yields force constants identical to those found in the AA structure, confirming that the slightly modified conformation seen in the AA mutant is not the cause of the increased flexibility. Its origin can rather be traced to the reduced side chain volumes in the mutant and notably that corresponding to the L212Glu → Ala substitution (which, in our representation, corresponds to the loss of a single side chain point). The position of this change within the overall protein structure is however crucial, since artificially introducing similar mutations at other positions within the protein can lead to very different effects. This is illustrated in Figures 5a and 5b, which show the results of modeling a mutation M234Glu → Ala, leading to smaller and less localized changes in the force constants and to both increased and decreased values.

DISCUSSION

The neutron scattering experiments carried out on the WT and nonfunctional mutant forms of the bacterial reaction center clearly indicate an overall increase in flexibility as a result of the point mutations. In the case of the backscattering experiments, this change is indicated by the increased slope of $\langle u^2 \rangle$ with temperature, above T_d. This change cannot be attributed to any particular part of the RC structure, although the identical behavior of both mutants (within the bounds of experimental error) suggests that the flexibility is increased as soon as L212Glu and L213Asp are mutated to Ala. For the TOF experiments, which address shorter timescales, a broadening of the $S(Q,\omega)$ spectrum is again observed above T_d, confirming increased flexibility. This technique shows no difference between the two mutants, although the $\langle u^2 \rangle$ backscattering measurements show a split in the curves above 240 K. This suggests that motions at an intermediate time scale (hundreds of picoseconds), specific to the mutants, make a significant contribution to the overall increase in flexibility. In terms of neutron scattering experiments, these results are the first evidence of an apparent decoupling

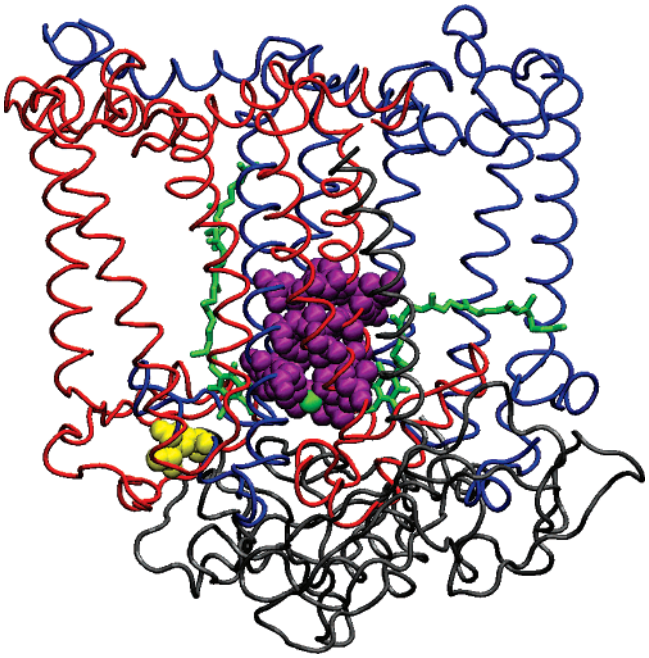

FIGURE 6: Ribbon diagram of the AA mutant form of RC showing the L (blue), M (red), and H (gray) subunits (pdb code 1K6N). The quinones Q_A (right) and Q_B (left) and the nonheme iron involved in protein function are shown in green. The mutated residues L212 and L213 are shown by the yellow van der Waals envelopes, and the residues showing the largest decrease in force constants (<-40 kcal mol^{-1} Å^{-2}), that is the largest increase in flexibility, as a result of the mutation are shown as purple van der Waals envelopes. The average distance between L212Glu and the residues shown in purple is above 15 Å.

between the increase of $\langle u^2 \rangle$ fluctuations, defining the dynamical transition, and the harmonic excess modes contained in the vibrational density of states and the boson peak (*13*).

The theoretical analysis of protein mechanics we have carried out is consistent with the experimentally observed increase in flexibility observed between the WT RC and the AA mutant. It suggests that this increase is largely due to the reduced side chain length associated with the L212Glu → Ala mutation. This change leads to increased flexibility in the core of the RC around the active site, although this region is relatively distant from the site of the point mutations.

It is noteworthy that L212Glu is systematically conserved in all photosynthetic bacteria (the L sequences of more than 70 species were aligned, as different as *R. sphaeroides*, *Allochromatium vinosum*, or *Roseobacter denitrificans* for example) (alignments made with ClustalW provided by EMBL). It can be concluded that L212Glu probably plays a special role although it is far from the main functional site. Interestingly, although L213Asp has been demonstrated to be of crucial importance for the delivery of the first proton to Q_B (*28*), it is much less conserved. Our present data suggest that if evolution has kept L212Glu in all bacteria it is probably not only for its role for proton transfer but very likely also for its involvement in maintaining protein rigidity.

From a more general point of view, we remark that the experimental and theoretical studies carried out here show that, at least in the case of the bacterial RC, nonfunctional mutants can be more flexible than a functional wild-type protein. Earlier modeling studies of a very different protein, cytochrome c peroxidase, also showed that its functional residues, in this case surrounding the catalytic heme iron, were more rigid in the active form of the protein (*14*). Taken together, these findings suggest that the common association of flexibility and function needs to be treated with caution. While environmental factors such as the temperature or the solvent can block function by preventing diffusion motions, it does not follow that loss of function necessarily implies less flexibility or, conversely, that functional residues will be among the most flexible within a protein. The present study points to the opposite conclusion and also shows that the effects of point mutations on protein flexibility can be surprisingly complex and long-range.

ACKNOWLEDGMENT

The authors wish to thank D.K. Hanson (Argonne National Laboratories) for many useful discussions, the Institut Laue Langevin for access to their neutron scattering facilities, and the CNRS for funding this research.

REFERENCES

1. Frauenfelder, H., Sligar, S. G., and Wolynes, P. G. (1991) The energy landscapes and motions of proteins, *Science 254*, 1598−603.
2. Elber, R., and Karplus, M. (1987) Multiple conformational states of proteins: a molecular dynamics analysis of myoglobin, *Science 235*, 318−21.
3. Daniel, R. M., Dunn, R. V., Finney, J. L., and Smith, J. C. (2003) The role of dynamics in enzyme activity, *Annu. Rev. Biophys. Biomol. Struct. 32*, 69−92.
4. Parak, F. G. (2003) Proteins in action: the physics of structural fluctuations and conformational changes, *Curr. Opin. Struct. Biol. 13*, 552−7.
5. Caliskan, G., Kisliuk, A., Tsai, A. M., Soles, C. L., and Sokolov, A. P. (2003) Protein dynamics in viscous solvents, *J. Chem. Phys. 118*, 4230−4236.
6. Cordone, L., Ferrand, M., Vitrano, E., and Zaccai, G. (1999) Harmonic behavior of trehalose-coated carbon-monoxy-myoglobin at high temperature, *Biophys. J. 76*, 1043−7.
7. Fitter, J., Lechner, R. E., Buldt, G., and Dencher, N. A. (1996) Internal molecular motions of bacteriorhodopsin: hydration-induced flexibility studied by quasielastic incoherent neutron scattering using oriented purple membranes, *Proc. Natl. Acad. Sci. U.S.A. 93*, 7600−5.
8. Zaccai, G. (2000) How soft is a protein? A protein dynamics force constant measured by neutron scattering, *Science 288*, 1604−7.
9. Reat, V., Patzelt, H., Ferrand, M., Pfister, C., Oesterhelt, D., and Zaccai, G. (1998) Dynamics of different functional parts of bacteriorhodopsin: H-2H labeling and neutron scattering, *Proc. Natl. Acad. Sci. U.S.A. 95*, 4970−5.
10. Hayward, J. A., and Smith, J. C. (2002) Temperature dependence of protein dynamics: computer simulation analysis of neutron scattering properties, *Biophys. J. 82*, 1216−25.
11. Tournier, A. L., and Smith, J. C. (2003) Principal components of the protein dynamical transition, *Phys. Rev. Lett. 91*, 208106.
12. Bartlett, G. J., Porter, C. T., Borkakoti, N., and Thornton, J. M. (2002) Analysis of catalytic residues in enzyme active sites, *J. Mol. Biol. 324*, 105−21.
13. Kurkal-Siebert, V., and Smith, J. C. (2006) Low-temperature protein dynamics: a simulation analysis of interprotein vibrations and the boson peak at 150 k, *J. Am. Chem. Soc. 128*, 2356−64.
14. Sacquin-Mora, S., and Lavery, R. (2006) Investigating the local flexibility of functional residues in hemoproteins, *Biophys. J. 90*, 2706−17.
15. Sacquin-Mora, S., and Lavery, R. (2007) Locating the active sites of enzymes using mechanical properties, *Proteins 67*, 350−359.
16. Tehei, M., Smith, J. C., Monk, C., Ollivier, J., Oettl, M., Kurkal, V., Finney, J. L., and Daniel, R. M. (2006) Dynamics of immobilized and native Escherichia coli dihydrofolate reductase by quasielastic neutron scattering, *Biophys. J. 90*, 1090−7.

17. Yang, L. W., and Bahar, I. (2005) Coupling between catalytic site and collective dynamics: a requirement for mechanochemical activity of enzymes, *Structure 13*, 893−904.
18. Yuan, Z., Zhao, J., and Wang, Z. X. (2003) Flexibility analysis of enzyme active sites by crystallographic temperature factors, *Protein Eng. 16*, 109−14.
19. Paddock, M. L., Feher, G., and Okamura, M. Y. (2003) Proton transfer pathways and mechanism in bacterial reaction centers, *FEBS Lett. 555*, 45−50.
20. Rutherford, A. W., and Faller, P. (2003) Photosystem II: evolutionary perspectives, *Philos. Trans. R. Soc. Lond. B Biol. Sci. 358*, 245−53.
21. Wraight, C. A. (2004) Proton and electron transfer in the acceptor quinone complex of photosynthetic reaction centers from Rhodobacter sphaeroides, *Front. Biosci. 9*, 309−37.
22. Ermler, U., Fritzsch, G., Buchanan, S. K., and Michel, H. (1994) Structure of the photosynthetic reaction centre from Rhodobacter sphaeroides at 2.65 Å resolution: cofactors and protein-cofactor interactions, *Structure 2*, 925−36.
23. Fritzsch, G., Koepke, J., Diem, R., Kuglstatter, A., and Baciou, L. (2002) Charge separation induces conformational changes in the photosynthetic reaction centre of purple bacteria, *Acta Crystallogr. Sect. D: Biol. Crystallogr. 58*, 1660−3.
24. Pokkuluri, P. R., Laible, P. D., Deng, Y. L., Wong, T. N., Hanson, D. K., and Schiffer, M. (2002) The structure of a mutant photosynthetic reaction center shows unexpected changes in main chain orientations and quinone position, *Biochemistry 41*, 5998−6007.
25. Stowell, M. H., McPhillips, T. M., Rees, D. C., Soltis, S. M., Abresch, E., and Feher, G. (1997) Light-induced structural changes in photosynthetic reaction center: implications for mechanism of electron-proton transfer, *Science 276*, 812−6.
26. Miksovska, J., Schiffer, M., Hanson, D. K., and Sebban, P. (1999) Proton uptake by bacterial reaction centers: the protein complex responds in a similar manner to the reduction of either quinone acceptor, *Proc. Natl. Acad. Sci. U.S.A. 96*, 14348−53.
27. Paddock, M. L., Rongey, S. H., Feher, G., and Okamura, M. Y. (1989) Pathway of proton transfer in bacterial reaction centers: replacement of glutamic acid 212 in the L subunit by glutamine inhibits quinone (secondary acceptor) turnover, *Proc. Natl. Acad. Sci. U.S.A. 86*, 6602−6.
28. Takahashi, E., and Wraight, C. A. (1990) A crucial role for AspL213 in the proton transfer pathway to the secondary quinone of reaction centers from Rhodobacter sphaeroides, *Biochim. Biophys. Acta 1020*, 107−111.
29. Tandori, J., Baciou, L., Alexov, E., Maroti, P., Schiffer, M., Hanson, D. K., and Sebban, P. (2001) Revealing the Involvment of Extended Hydrogen-Bond Networks in the Cooperative Function between Distant Sites in Bacterial Centers, *J. Biol. Chem. 276*, 45513−15.
30. Hanson, D. K., Tiede, D. M., Nance, S. L., Chang, C. H., and Schiffer, M. (1993) Site-specific and compensatory mutations imply unexpected pathways for proton delivery to the QB binding site of the photosynthetic reaction center, *Proc. Natl. Acad. Sci. U.S.A. 90*, 8929−33.
31. Hanson, D. K., Baciou, L., Tiede, D. M., Nance, S. L., Schiffer, M., and Sebban, P. (1992) In bacterial reaction centers protons can diffuse to the secondary quinone by alternative pathways, *Biochim. Biophys. Acta 1102*, 260−5.
32. Gall, A., Seguin, J., Robert, B., and Bellissent-Funel, M. C. (2002) Membrane Proteins in Bulk Solution Can Be Used for Quasi-Elastic Neutron Scattering Studies: The Case for the Photochemical Reaction Center, *J. Phys. Chem. B 106*, 6303−6309.
33. Zacharias, M. (2003) Protein-protein docking with a reduced protein model accounting for side-chain flexibility, *Protein Sci. 12*, 1271−82.
34. Atilgan, A. R., Durell, S. R., Jernigan, R. L., Demirel, M. C., Keskin, O., and Bahar, I. (2001) Anisotropy of fluctuation dynamics of proteins with an elastic network model, *Biophys. J. 80*, 505−15.
35. Doruker, P., Jernigan, R. L., and Bahar, I. (2002) Dynamics of large proteins through hierarchical levels of coarse-grained structures, *J. Comput. Chem. 23*, 119−27.
36. Berman, H. M., Battistuz, T., Bhat, T. N., Bluhm, W. F., Bourne, P. E., Burkhardt, K., Feng, Z., Gilliland, G. L., Iype, L., Jain, S., Fagan, P., Marvin, J., Padilla, D., Ravichandran, V., Schneider, B., Thanki, N., Weissig, H., Westbrook, J. D., and Zardecki, C. (2002) The Protein Data Bank, *Acta Crystallogr. Sect. D: Biol. Crystallogr. 58*, 899−907.
37. Cusack, S., and Doster, W. (1990) Temperature dependence of the low frequency dynamics of myoglobin. Measurement of the vibrational frequency distribution by inelastic neutron scattering, *Biophys. J. 58*, 243−51.
38. Xu, Q., and Gunner, M. R. (2001) Trapping conformational intermediate states in the reaction center protein from photosynthetic bacteria, *Biochemistry 40*, 3232−3241.
39. Diehl, M., Doster, W., Petry, W., and Schober, H. (1997) Water-coupled low-frequency modes of myoglobin and lysozyme observed by inelastic neutron scattering. *Biophys. J. 73*, 2726−32.
40. Giordano, R., Grasso, A., Teixeira, J., Wanderlingh, F., and Wanderlingh, U. (1991) Small-angle neutron scattering in lysozyme solutions, *Phys. Rev. A 43*, 6894−6899.
41. Smith, J., Kuczera, K., and Karplus, M. (1990) Dynamics of myoglobin: comparison of simulation results with neutron scattering spectra, *Proc. Natl. Acad. Sci. U.S.A. 87*, 1601−5.
42. Bicout, D. J., and Zaccai, G. (2001) Protein Flexibility from the Dynamical Transition: A Force Constant Analysis, *Biophys. J. 80*, 1115−23.
43. Kurkal, V., Daniel, R. M., Finney, J. L., Tehei, M., Dunn, R. V., and Smith, J. C. (2005) Low frequency enzyme dynamics as a function of temperature and hydration: A neutron scattering study. *Chem. Phys. 317*, 267−73.
44. Begen, B., Kisliuk, A., Novikov, V., Sokolov, A., Niss, K., Chauty-Cailliaux, A., Alba-Simionesco, C., and Frick, B. (2006) Influence of pressure on fast dynamics in polyisobutylene, *J. Non-Cryst. Solids* (in press).
45. Frick, B., and Alba-Simionesco, C. (1999) Comparison of the pressure and temperature dependence of the elastic incoherent scattering for the polymers polybutadiene and polyisobutylene, *Phys. B 266*, 13−19.
46. Frick, B., and Alba-Simionesco, C. (2002) Pressure dependence of the Boson peak in poly (butadiene), *Appl. Phys. A 74*.
47. Leonforte, F., Tanguy, A., Wittmer, J. P., and Barrat, J. L. (2006) Inhomogeneous elastic response of silica glass, *Phys. Rev. Lett. 97*, 055501.
48. Lubchenko, V., and Wolynes, P. G. (2003) The origin of the boson peak and thermal conductivity plateau in low-temperature glasses, *Proc. Natl. Acad. Sci. U.S.A. 100*, 1515−8.
49. Monaco, A., Chumakov, A. I., Monaco, G., Crichton, W. A., Meyer, A., Comez, L., Fioretto, D., Korecki, J., and Ruffer, R. (2006) Effect of Densification on the Density of Vibrational States of Glasses, *Phys. Rev. Lett. 97*.
50. Niss, K., and Alba-Simionesco, C. (2006) Effect of density and temperature on correlations between fragility and glassy properties, *Phys. Rev. B 74*, 024205.
51. Schirmacher, W., Ruocco, G., and Scopigno, T. (2007) Acoustic Attenuation in Glasses and its Relation with the Boson Peak, *Phys. Rev. Lett. 98*, 25501.
52. Brown, K. G., Erfurth, S. C., Small, E. W., and Peticolas, W. L. (1972) Conformationally dependent low-frequency motions of proteins by laser Raman spectroscopy, *Proc. Natl. Acad. Sci. U.S.A. 69*, 1467−9.
53. Fenimore, P. W., Frauenfelder, H., McMahon, B. H., and Young, R. D. (2004) Bulk-solvent and hydration-shell fluctuations, similar to alpha- and beta-fluctuations in glasses, control protein motions and functions, *Proc. Natl. Acad. Sci. U.S.A. 101*, 14408−13.
54. Ferrand, M., Dianoux, A. J., Petry, W., and Zaccai, G. (1993) Thermal motions and function of bacteriorhodopsin in purple membranes: effects of temperature and hydration studied by neutron scattering, *Proc. Natl. Acad. Sci. U.S.A. 90*, 9668−72.
55. Fitter, J. (1999) The temperature dependence of internal molecular motions in hydrated and dry alpha-amylase: the role of hydration water in the dynamical transition of proteins, *Biophys. J. 76*, 1034−42.
56. Paciaroni, A., Stroppolo, M. E., Arcangeli, C., Bizzarri, A. R., Desideri, A., and Cannistraro, S. (1999) Incoherent neutron scattering of copper azurin: a comparison with molecular dynamics simulation results, *Eur Biophys. J. 28*, 447−56.
57. Roh, J. H., Curtis, J. E., Azzam, S., Novikov, V. N., Peral, I., Chowdhuri, Z., Gregory, R. B., and Sokolov, A. P. (2006) Influence of hydration on the dynamics of lysozyme, *Biophys. J. 91*, 2573−88.
58. Daniel, R. M., Finney, J. L., Réat, V., Dunn, R., Ferrand, M., and Smith, J. C. (1999) Enzyme Dynamics and Activity: Time-Scale Dependence of Dynamical Transitions in Glutamate Dehydrogenase Solution, *Biophys. J. 77*, 2184−90.

59. Gabel, F., Weik, M., Doctor, B. P., Saxena, A., Fournier, D., Brochier, L., Renault, F., Masson, P., Silman, I., and Zaccai, G. (2004) The Influence of Solvent Composition on Global Dynamics of Human Butyrylcholinesterase Powders: A Neutron-Scattering Study, *86*, 3152−65.
60. Tirion, M. M. (1996) Large Amplitude Elastic Motions in Proteins from a Single-Parameter, Atomic Analysis, *Phys. Rev. Lett. 77*, 1905−1908.
61. Tozzini, V. (2005) Coarse-grained models for proteins, *Curr. Opin. Struct. Biol. 15*, 144−50.
62. Zachariae, U., and Lancaster, C. R. (2001) Proton uptake associated with the reduction of the primary quinone Q(A) influences the binding site of the secondary quinone Q(B) in Rhodopseudomonas viridis photosynthetic reaction centers, *Biochim. Biophys. Acta 1505*, 280−90.
63. Baciou, L., and Sebban, P. (1995) Heterogeneity of the quinone electron acceptor system in bacterial reaction centers, *Photochem. Photobiol. 62*, 271−278.
64. Spitz, J. A., Derrien, V., Baciou, L., and Sebban, P. (2005) Specific triazine resistance in bacterial reaction ceters induced by a single mutation in the QA protein pocket, *Biochemistry 44*, 1338−43.
65. Frick, F., Combet, J., Pfister, C. (2001) Neutron backscattering and its application in soft matter investigation, *J. Phys. Soc. Jpn. 70* (Suppl. A), 311−316.
66. Gabel, F. (2006) Protein dynamics in solution and powder measured by incoherent elastic neutron scattering: the influence of Q-range and energy resolution, *Eur. Biophys. J. 34*, 1−12.

BI7004416